Properties of an optical soliton gas

A. Schwache and F. Mitschke*
Institut für Angewandte Physik, Universität Münster, Corrensstrasse 2/4, D-48149 Münster, Germany
(Received 18 November 1996)

We consider light pulses propagating in an optical fiber ring resonator with anomalous dispersion. New pulses are fed into the resonator in synchronism with its round-trip time. We show that solitary pulse shaping leads to a formation of an ensemble of subpulses that are identified as solitons. All solitons in the ensemble are in perpetual relative motion like molecules in a fluid; thus we refer to the ensemble as a soliton gas. Properties of this soliton gas are determined numerically. [S1063-651X(97)08406-7]

PACS number(s): 42.65.Tg, 42.65.Sf, 42.81.Dp

INTRODUCTION

It is well known that in a variety of nonlinear wave propagation processes there exist pulses with special properties and special shape called solitons. Solitons can form from initial conditions that can be quite different from their eventual shape. They can collide and pass through each other without being destroyed; this was noted in [1] and lead to their name, which implies a particlelike property. In fiber optics, in particular, solitons are the natural bits of information for long-distance transmission, a conclusion that has considerable impact on future telecommunication technology.

Wave propagation in optical fiber is well understood; see, e.g., the book by Agrawal [2]. One has to take into account group velocity dispersion and self-phase modulation. The former is usually written as a power series in frequency separation from the central frequency of the light; in many cases it suffices to consider what is known as second-order dispersion, commonly expressed as the parameter β_2. The latter is caused by what is often referred to as the optical Kerr effect: The index of refraction n of silica fiber is given by $n=n_0+n_2 I$, where n_0 is the small signal index familiar from classical optics, I is the light intensity, and n_2 is the Kerr coefficient, which here takes values around 3×10^{-20} m^2/W. Note that this expression implies an instantaneous response of the medium, which is a reasonable approximation for pulses much longer than the Raman time T_R, which is of the order of 10^{-14} s.

The influence of both β_2 and n_2 is captured in the celebrated nonlinear Schrödinger equation (NLSE)

$$i\frac{\partial A}{\partial z}=\frac{1}{2}\beta_2\frac{\partial^2 A}{\partial T^2}-\gamma|A|^2A. \tag{1}$$

A refers to the envelope of the electrical field, z is distance, and T is local time. $\gamma=n_2\omega_0/cA_{\rm eff}$ is the nonlinearity coefficient; herein ω_0 is the optical frequency and $A_{\rm eff}$ the effective mode cross-sectional area. Depending on the desired degree of approximation, the NLSE is often enhanced with further terms describing fiber losses, higher-order dispersion, or the delay T_R of the response of the medium that leads to Raman scattering. In what follows, we will add on the right-hand side the terms $(i/6)\beta_3\partial^3A/\partial T^3$ for third-order dispersion. We emphasize, though, that this correction is added solely to make the correspondence to our experiment as close as possible; the essentials of the phenomena described here occur in their absence just as well.

It is well known that the NLSE exhibits a constant shape solution of the form

$$A(z,T)=\sqrt{P_1}\,\mathrm{sech}\frac{T}{T_0}\exp\left(\frac{i}{2L_D}z\right), \tag{2}$$

which is called the fundamental soliton. It has a pulse width T_0 and peak power $P_1=1/\gamma L_D$. $L_D=T_0^2/|\beta_2|$ is a characteristic dispersion length.

There also exists an infinite family of higher-order solitons of integer order N (N-soliton bound states) with $P_N=N^2P_1$. The shapes of all higher-order integer order N solitons oscillate and repeat after the soliton period $z_0=(\pi/2)L_D$.

The ability of fiber solitons to form from initial nonsoliton pulses and acquire their characteristic shape was observed experimentally in [3]. An experimental observation of the soliton interaction was reported in [4], where pairs of copropagating solitons were studied. However, it stands to reason that whatever applications may evolve one day, they will presumably deal with many more than just two solitons. In this paper we will consider an ensemble of solitons, all of which can interact. There is a considerable amount of literature on such a situation in various fields such as plasma physics [5] and solid-state physics [6] under the name of a ''soliton gas.'' However, with few exceptions [7,8], this literature is theoretical. For fiber optics in particular there are a few theoretical papers [9–11], but no experiments have been reported. Falling just short of presenting actual experimental data, we present an experiment in which a ''soliton gas'' does form; unfortunately, the ultrashort time scales involved have made it unfeasible so far to ''see'' it directly. However, we will study its statistical properties by numerical simulation.

*FAX: 49-251-83-33513.
Electronic address: mitschk@uni-muenster.de

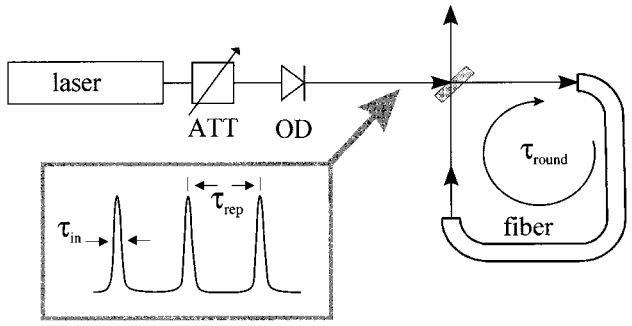

FIG. 1. Schematic of the experimental setup. Laser, cw mode-locked laser; ATT, variable attenuator; OD, optical diode (Faraday isolator, prevents feedback into the laser); fiber, typically 10 m of single-mode polarization-preserving fiber. The inset defines the pulse width τ_{in} and the repetition time τ_{rep}. Resonator round-trip time is denoted by τ_{round}. For synchronous drive, $\tau_{rep}=\tau_{round}$.

I. EXPERIMENT

Consider a piece of single-mode fiber closed onto itself such as to form a ring resonator. Feed this resonator at some input coupler with pulses of light of duration τ_{in}, which is much shorter than the resonator round-trip time τ_{round} (typically, τ_{in} will be a few picoseconds and τ_{round} several nanoseconds). Also, arrange for the repetition time τ_{rep} of the external drive pulses to be equal to the round-trip time. In other words, consider a synchronously driven fiber ring resonator. A sketch of the experimental setup is shown in Fig. 1. For further detail, see Refs. [12–14].

Propagation around the ring is described by the NLSE as above. The additional ingredient now is the interference between a pulse inside the ring with an external feed pulse once every round-trip time. Owing to the self-phase modulation acting on the pulse in the fiber it will acquire a chirp; upon interference, this chirp will translate into amplitude effects. For example, whenever the phase of both interfering pulses match constructively the resulting pulse will have a peak, whereas in positions of opposite phase the resulting pulse will have a notch due to destructive interference.

As has been described before [15], the pulses traveling in the ring will acquire complicated shapes after only a few round-trips. This has been studied under conditions of normal dispersion and was shown to give rise to optical turbulence. It was also shown that a measure of the complexity of the shapes is given by the ''system size'' [13,14]. This quantity is determined by the ratio of two widths: the width of the feed pulses divided by the typical width of the narrow substructures emerging from the process. The latter in turn equals the correlation width set by the amount of dispersion. The situation may be compared loosely to that of hydrodynamic turbulence, where an upper length scale of eddies is set by the container size and a lower length scale by viscosity.

In the present paper we concentrate on the case where the fiber has anomalous dispersion. We find that now individual, isolated narrow subpulses emerge from the feed pulse. Figure 2 shows a typical situation. Superimposed is the feed pulse for comparison. Evidently, the substructure can exist only within the width of the feed pulse.

We will proceed by first demonstrating that the subpeaks

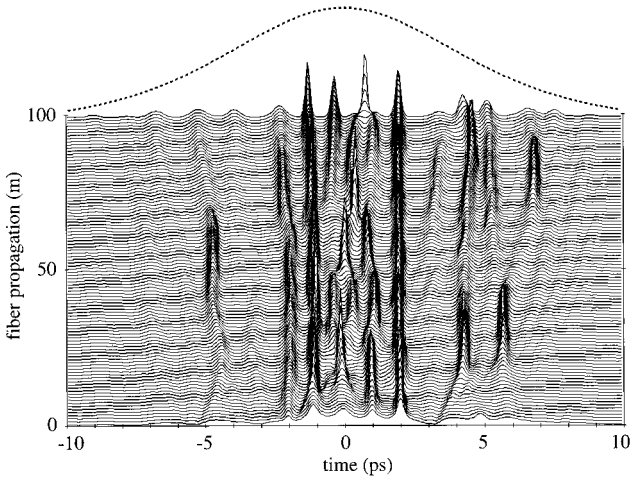

FIG. 2. Feed pulse and substructure are shown over one round-trip around the nonlinear ring resonator or 100-m fiber. 200 round-trips were preiterated, during which the feed pulse (shown as a dotted line with exaggerated vertical scale for comparison) has reshaped into an ensemble of subpulses. Parameters: input peak power $P_{in}=80$ W, input pulse width $\tau_{in}=10$ ps; dispersion: $\beta_2=-10$ ps^2/km, $\beta_3=-0.135$ ps^3/km.

are indeed solitonlike. Then we will discuss how many such solitary pulses can emerge. Finally, we will look at the density and the kinetics of the subpulses.

II. NUMERICAL EXPERIMENT

Since the ultrafast time scales involved make a direct measurement on a single shot basis extremely difficult, we have to resort to a numerical simulation for now. The present investigation is based on a split-step Fourier calculation similar to that in [2]. We typically used spatial steps of 5 cm and 1024 time steps for a total time window of, e.g., 50 ps for 10-ps pulses. Periodic boundary conditions were used; energy conservation were monitored to guard against numerical inaccuracies. For the data discussed below, 200 round-trips were preiterated to let any initial transients die out. Then 1000 more round-trips were calculated; this constitutes the database to which all analysis below will refer.

First we extract the position, peak power, and width of all maxima as a function of time. To find the position and peak power is a straightforward routine. The determination of the width requires a remark: Since it is common in experiments to describe pulses by their half-width τ full width at half maximum rather than by T_0, we use a routine that searches the half maximum points on either side of each maximum to obtain the width τ. Occasionally, two subpeaks are so close to each other that this strategy fails; in such cases we make no further attempt to determine τ. It turns out that some maxima are detected mostly in the wings of the whole structure that are really just small ripples in the power profile (compare Fig. 2).

A. Subpeaks are solitonlike

Under the conditions chosen, the prominent maxima have typical peak powers of $P=40$–200 W and typical widths around $\tau=600$–1600 fs. It is also quite obvious that the

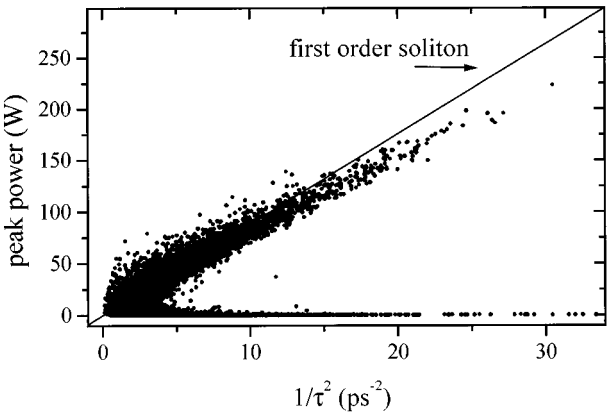

FIG. 3. Diagram of correlation between peak power and width of subpulses. Only subpulses with peak power greater 0.5 W are taken into account. Parameters: input peak power $P_{\mathrm{in}}=40$ W, others as in Fig. 2. The solid line is the theoretical expectation for the fundamental soliton [Eq. (3)].

highest peaks tend to be the narrowest. This anticorrelation is shown in Fig. 3, where P is plotted over τ^{-2}. One easily identifies two branches. The majority of data points is at very low values of P and can have any value of τ^{-2} over the range shown and larger. This branch consists of linear waves and numerical noise. The other branch corresponds to nonlinear pulses and displays a linear trend so that $P\tau^2\approx$const. The solid line, shown for comparison, represents the combinations of P and τ that one expects for an unperturbed fundamental (i.e., $N=1$) soliton. This line is not a fit to the data; there are no free parameters. The peak power of the fundamental soliton is given by

$$P_1=C_{\mathrm{sech}}\frac{|\beta_2|}{\gamma\tau^2}, \tag{3}$$

where the numerical factor $C_{\mathrm{sech}}=4\ln^2(1+\sqrt{2})\approx 3.11$ originates from the sech^2-like power profile. It is quite apparent that the nonlinear pulses fall close to this line; this justifies the identification of these pulses as solitonlike.

A different way to display these data is to introduce the soliton order N through $P_N=N^2P_1$ into Eq. (3) and solve for N. Then, from the width τ and peak height P of the pulses we can empirically determine an estimate of the soliton order, which we call N^*, as

$$N^*=\sqrt{\frac{P}{P_1}}=\sqrt{\frac{\gamma P\tau^2}{C_{\mathrm{sech}}|\beta_2|}}. \tag{4}$$

A fundamental soliton should have $N^*\approx N=1$ all the time. Other pulses will have different values, and as their shapes change, so will N^*. However, whenever their shape is reasonably close to sech^2, the identification of N^* and N is reasonable.

Figure 4 shows a histogram of all N^* values encountered over 1000 round-trips; the peaking at $N^*=1$ is unmistakeable. The other peak at $N^*=0$ is due to linear pulses; for the sake of clarity we will from now on cut their number by disregarding maxima with a peak power not exceeding 2 W.

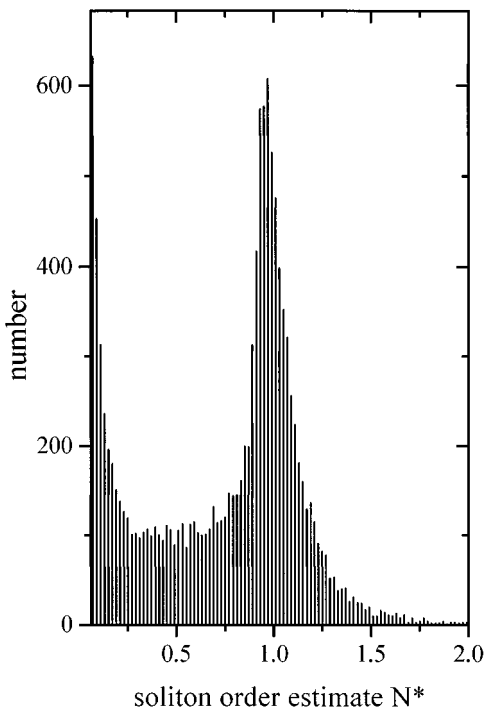

FIG. 4. Histogram for the soliton order estimate N^* obtained from 1000 round-trips. Same data and parameters as in Fig. 3.

We conclude that the pulses, while perturbed strongly, eventually settle to a fundamental soliton, as evidenced by the correlation of pulse width and peak power. Since there is a considerable spread in both widths and peak powers, we proceed to look at the distributions of these quantities. Also, since we deal with a whole ensemble of pulses, we look at their number and mutual distance.

B. Distribution of peak power of solitons

In the following section, we are repeatedly faced with the problem that linear and nonlinear pulses exhibit different properties so that statistical measures, taken blindly, represent an ill-defined mixture. We therefore attempt to separate both ''populations'' by defining a threshold criterion: Pulses with $N^*>1/2$ are identified as nonlinear; only these will be considered further. Note, however, that a complete separation is not feasible because both populations merge at low powers and become undistinguishable by this criterion. Due to this imperfect separation, linear pulses still contribute a very high and rather narrow peak at fairly low power in the histogram of peak powers (see Fig. 5). Beyond the crossover to the nonlinear pulses, the histogram decays exponentially, as evidenced by the linear decay in the semilogarithmic plot of Fig. 3. It means that very powerful pulses are rare.

C. Distribution of width of solitons

The histogram of the pulse widths is shown in Fig. 6. Again, for large widths there is an exponential decay indicating that very wide pulses are very rare. On the other hand, very narrow pulses are also very rare, which is not too surprising because very powerful pulses were shown above to

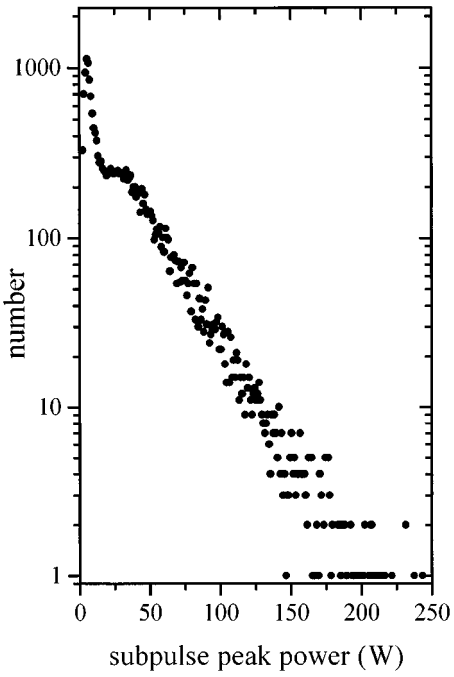

FIG. 5. Histogram for the subpulse peak power. From 2000 round-trips all subpulses with peak power greater 2 W and with a soliton order estimate $N^* > 0.5$ were taken into account. The parameters are the same as in Fig. 3.

be very rare too. The overall shape of the histogram resembles a distribution $P(\tau) = a\tau^3 \exp(-\tau/b)$ with a, b fit constants (formally, a Planck distribution), shown as a solid line and intended merely to guide the eye.

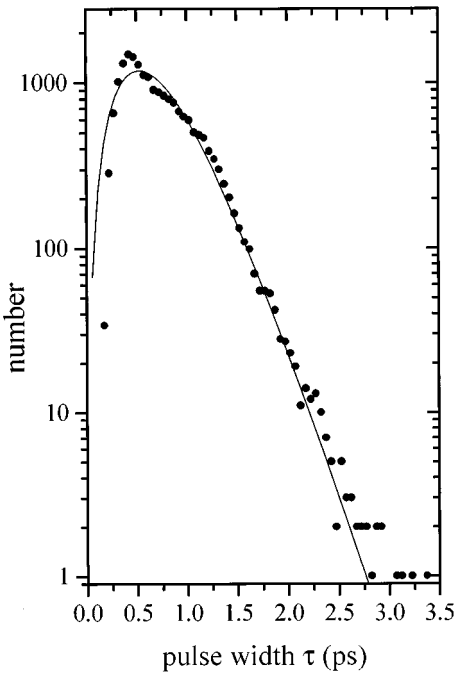

FIG. 6. Histogram for the subpulse width τ. Same data as in Fig. 5. The solid line guides the eye (see the text).

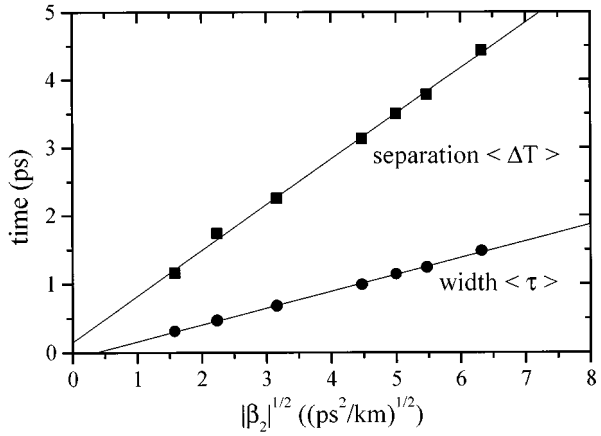

FIG. 7. Mean values for the pulse width τ and the distance ΔT between the subpulses during the fiber propagation for different values of β_2. Other parameters are the same as in Fig. 5.

D. Scaling of the separation of solitons

It was pointed out above that the width of the solitons scales with dispersion according to $\tau \propto \sqrt{|\beta_2|}$. Figure 7 shows this relation for the average pulse width $\langle \tau \rangle$. Evaluation of the separation between neighboring solitons reveals that within the accuracy of the fit there is the same type of scaling: Fig. 7 shows the average separation $\langle \Delta T \rangle$ plotted versus $\sqrt{|\beta_2|}$. Thus the *relative* pulse separation (in units of pulse width) does not depend on dispersion. The dependence of $\langle \tau \rangle$ and $\langle \Delta T \rangle$ on the input power is shown in Fig. 8; again, there is a linear relation with $P^{-1/2}$ for both $\langle \tau \rangle$ and $\langle \Delta T \rangle$, while the relative pulse separation varies only slightly.

E. Distribution of the separation of solitons

The histogram of the separation between neighboring pulses looks very similar to the pulse width histogram (Fig. 9). In fact, we use the same type of function for the solid line to guide the eye. Very wide pulse spacing is improbable and so is a very close distance. This is a significant deviation from a purely random distribution of pulses over the avail-

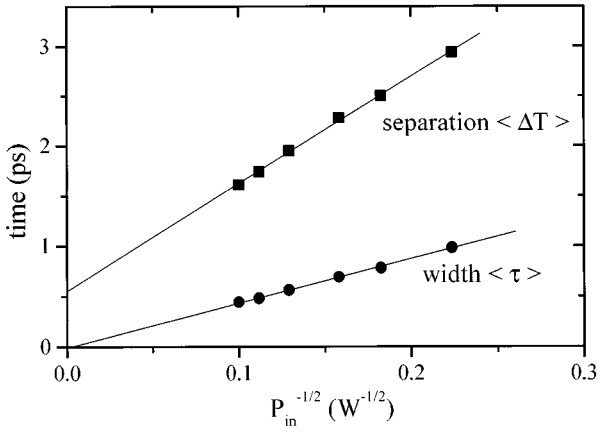

FIG. 8. Mean values for the pulse width τ and the distance ΔT between the subpulses during the fiber propagation for different values of input power P_{in}. Other parameters are the same as in Fig. 5.

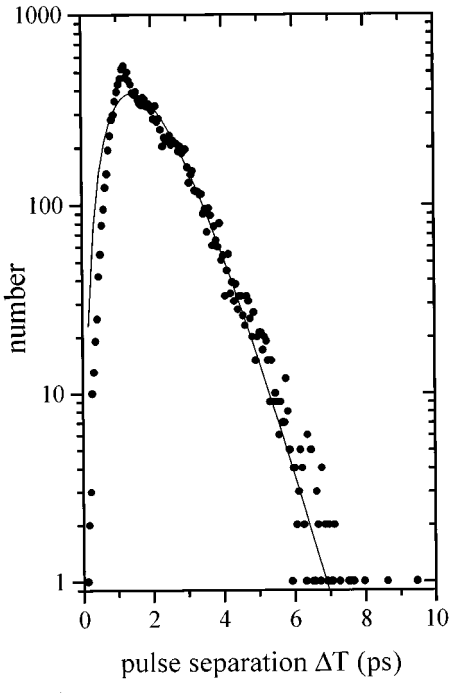

FIG. 9. Histogram for the subpulse separation ΔT over 1000 round-trips. Same data as in Fig. 5. The solid line guides the eye (see the text).

able interval; the latter would result in a monotonic (approximately exponential) distribution, whereas the actual distribution clearly has a maximum.

One might have the suspicion that the maximum could be an artifact due to difficulties of counting all pulse pairs correctly when the separation between neighboring pulses becomes smaller than the width of the participating pulses. We checked this by creating the corresponding histogram of distances for only those pulses that have a pulse width of less than 0.3 ps. The maximum of the distribution remained at 1.2 ps, so that such an artifact can be ruled out.

F. Number of solitons

Figure 2 graphically illustrates the development of a pulse during the fiber propagation over one round-trip, starting right after interference. Evidently, not only are the shape and position of solitary subpulses subject to fluctuations, but so is their number. Figure 10 shows that the number $\langle n \rangle$ changes not only during interference, but also during propagation. The average number $\langle n \rangle$ (where the average is taken over many round-trips) is essentially determined by their separation and the available width, the latter given by the feed pulse width, in the same spirit as the number of substructures is given by the system size (see above and [13,14]).

We test this assumption by varying the input pulse width and tracking $\langle n \rangle$ at the end of each round-trip. First, we control the system size by varying β_2; it is expected to scale as $\sqrt{\beta_2}$ [13,14]. As Fig. 10 shows, there is indeed the expected behavior. Second, we control the system size by way of varying the input pulse width; with all other parameters kept constant, it increases linearly with τ_{in}. Figure 11 shows the result: Indeed, $\langle n \rangle$ grows linearly with τ_{in}. One concludes that the average separation between subpulses must

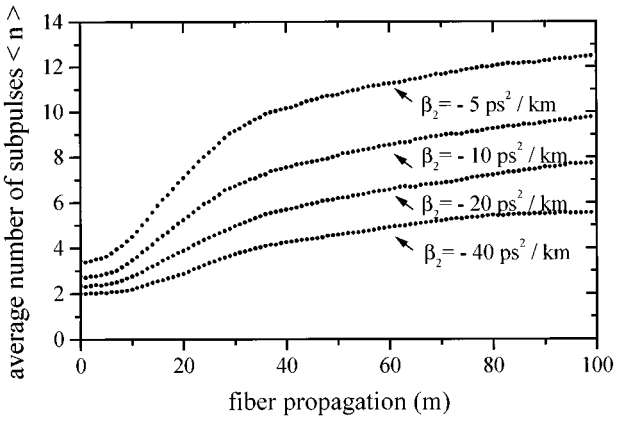

FIG. 10. Mean number of subpulses during the fiber propagation for four different values of β_2. Other parameters are the same as in Fig. 5.

remain essentially constant as long as β_2 is constant; this is corroborated by Fig. 7.

III. SOLITON FLUID

We have so far considered the ensemble of solitonlike pulses with respect to their static properties. In fact, the whole ensemble is in constant motion, much like the atoms in a fluid. In keeping with terminology in the literature, we therefore refer to the ensemble as a soliton gas. (Note, however, that in the absence of compressibility data the distinction between a gas and a liquid is not obvious.)

We have stated how the (average) number of ''particles'' in this gas determined. By using the average separation given above, we can also define the density $\rho = \langle \Delta T \rangle^{-1/D}$, where D is a dimension and in this case the dimension of the embedding space $D=1$. We have preliminary data indicating that from the relative motion of the solitons, also a ''temperature'' can be defined that depends on the pump power. Further characterization of the soliton gas in the spirit of thermodynamics and statistical mechanics must be left for future work.

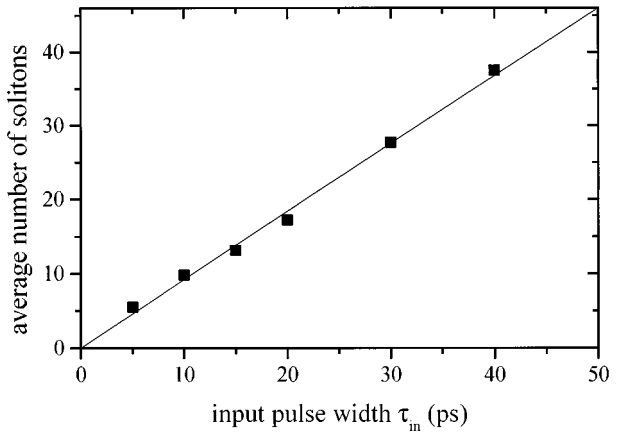

FIG. 11. Mean number of subpulses for different input pulse width. Other parameters are the same as in Fig. 5.

IV. CONCLUSION

We have described an experimental situation in which an ensemble of subpulses is created from a broader input pulse. Individual subpulses have been shown to be solitons. The ensemble as a whole is in constant motion, suggesting a fluid of particles: hence the term soliton gas. Direct experimental verification will be very challenging in view of the very short time scales involved and the necessity of single-shot observation. Meanwhile, numerical investigation provides detailed statistical material on the properties of such gas. The soliton gas provides a unique opportunity to study the interactions between a large number of solitons.

ACKNOWLEDGMENTS

We have enjoyed discussions with N. Akhmediev, C. Etrich, F. Lederer, and B. Malomed. This work was financially supported by Deutsche Forschungsgemeinschaft.

[1] N. J. Zabusky and M. Kruskal, Phys. Rev. Lett. **15**, 240 (1965).
[2] G. P. Agrawal, *Nonlinear Fiber Optics* (Academic, San Diego, 1995).
[3] L. F. Mollenauer, R. H. Stolen, and J. P. Gordon, Phys. Rev. Lett. **45**, 1095 (1980).
[4] F. M. Mitschke and L. F. Mollenauer, Opt. Lett. **12**, 955 (1987).
[5] Mei-Mei Shen and D. R. Nicholson, Phys. Fluids **30**, 1096 (1987).
[6] H. Büttner and F. G. Mertens, Solid State Commun. **29**, 663 (1979).
[7] L. A. Ostrovskii, Radiophys. Quantum Electron. **19**, 464 (1976).
[8] S. E. Nagler, W. J. L. Buyers, R. L. Armstrong, and B. Briat, Phys. Rev. B **28**, 3873 (1983).
[9] B. A. Malomed, Phys. Rev. A **41**, 4538 (1990).
[10] B. A. Malomed, Europhys. Lett. **30**, 507 (1995).
[11] I. M. Uzunov, R. Muschall, M. Gölles, F. Lederer, and S. Wabnitz, Opt. Commun. **118**, 577 (1995).
[12] G. Steinmeyer, A. Buchholz, M. Hänsel, M. Heuer, A. Schwache, and F. Mitschke, Phys. Rev. A **52**, 830 (1995).
[13] G. Steinmeyer and F. Mitschke, Appl. Phys. B **62**, 367 (1996).
[14] F. Mitschke, G. Steinmeyer, and A. Schwache, Physica D **96**, 251 (1996).
[15] F. Mitschke, G. Steinmeyer, M. Heuer, A. Schwache, and I. Klopsch, in *Coherence and Quantum Optics 7*, edited by J. Eberly, L. Mandel, and E. Wolf (Plenum, New York, 1996), p. 457.